International Journal of Applied Pharmaceutics

ISSN- 0975-7058 Vol 17, Issue 6, 2025

Original Article

DEVELOPMENT AND EVALUATION OF SILVER NANOPARTICLES-LOADED PHYTOGEL OF HYDROALCOHOLIC EXTRACT OF *FICUS VIRENS* BARK: FORMULATION, OPTIMIZATION, AND ANTIMICROBIAL EFFICACY

DEEPIKA AGGARWAL, KAMAL SAROHA*, MANJUSHA CHOUDHARY*, KAMAL KAUSHIK

Institute of Pharmaceutical Sciences, Kurukshetra University, Kurukshetra, Haryana-136119, India
***Corresponding author: Kamal Saroha; *Email: kamal@kuk.ac.in**

Received: 04 Aug 2025, Revised and Accepted: 03 Oct 2025

ABSTRACT

Objective: This study aimed to develop, optimize, and characterize a transdermal phytogel incorporating silver nanoparticles (AgNPs) loaded with *Ficus virens* hydroalcoholic bark extract, using Carbopol 940 as the gelling agent, to enhance antimicrobial efficacy and formulation stability.

Methods: This research involved the preparation of phytogel formulations by systematically varying the concentrations of Carbopol 940 and silver nanoparticles combined with hydroalcoholic *Ficus virens* bark extract (*FV-BE*). A Central composite design (CCD) was employed to optimize the formulations and evaluate the influence of independent factors on key formulation attributes. Comprehensive physicochemical evaluations, including measurements of pH, viscosity, spreadability, extrudability, drug content, entrapment efficiency, and stability, are conducted to ensure suitability for topical application. The nanoparticulate system was described *via* zeta potential, particle size, and polydispersity index (PDI) study. To further understand the release mechanisms, *in vitro* drug release and kinetic modeling were performed. The agar well diffusion method was used to evaluate the antibacterial activity against *Aspergillus niger, Pseudomonas aeruginosa, Staphylococcus aureus*, *and Escherichia coli.*

Results: The optimized formulation (F7) containing 0.75% w/w Carbopol 940 and 0.02% w/w AgNPs with *FV-BE* exhibited desirable physicochemical properties, including suitable viscosity (5517±1.2 cps), spreadability (12.75±1.67 g. cm/s), pH (6.64±0.097), high entrapment efficiency (90.23±0.37%), and drug content (92.95%±1.12%). The average particle size was 259.5 nm with a PDI of 0.280, and the zeta potential was -26.5 mV, indicating moderate colloidal stability. *In vitro* drug release studies revealed a complete diffusion-controlled release over 24 h, fitting the Korsmeyer-Peppas model with a non-Fickian diffusion mechanism. The phytogel formulation demonstrated notable antimicrobial activity against *Escherichia coli, Staphylococcus aureus, Pseudomonas aeruginosa*, and *Aspergillus niger*, with inhibition zones comparable to standard antibiotics. Stability studies confirmed the formulation's robustness under various storage conditions over three months.

Conclusion: The developed phytogel incorporating *FV-BE* and AgNPs is a promising nanocarrier-based system for effective topical antimicrobial therapy. Further *in vivo* and clinical validations are warranted to advance its therapeutic application.

Keywords: Silver nanoparticles, Phytogel, Herbal extract, Antimicrobial activity, Topical formulation, Green synthesis, Optimization, Agar well diffusion

DOI: https://dx.doi.org/10.22159/ijap.2025v17i6.56393 Journal homepage: https://innovareacademics.in/journals/index.php/ijap

INTRODUCTION

Gels are widely utilized in topical dosage forms and lubricants owing to their favorable application properties. Fundamentally, gels consist of a liquid medium in which other constituents are dispersed to form a semi-solid network. These formulations are designed for application on the skin or mucosal surfaces to deliver localized therapeutic effects or enable transdermal absorption of active agents [1]. In addition to their medicinal roles, gels may provide protective or emollient functions. Drug release from gels typically resembles that of simple solutions, as the polymeric network permits the free diffusion of drug molecules through the continuous liquid phase [2]. Furthermore, transdermal gel systems can be engineered to sustain drug release, thereby maintaining steady systemic drug concentrations over extended periods [3].

Structurally, gels tend to be firmer than jellies because of the stronger covalent cross-linking and a higher number of physical bonds within the polymer framework [4]. Compared with transdermal patches, gels offer advantages such as flexible dosing, reduced potential for skin irritation, and improved patient compliance owing to their pleasing appearance and ease of use [5]. The appearance of gels can range from fully transparent to somewhat cloudy, depending on the molecular solubility of the constituents or aggregation, which causes light scattering. Typically, the gelling agent concentration is maintained below 10%, optimally between 0.5% and 2.0%, to form stable gels [6].

Gels are physically formed when large amounts of water are entrapped within a three-dimensional network, differentiating them from creams or ointments. This high-water content enhances the drug solubility and promotes the diffusion of active compounds. However, the delivery of hydrophobic drugs *via* gels is challenging because of their poor water solubility, which limits their effective delivery through conventional gel bases [7]. Phytogels have attracted considerable interest in overcoming these limitations.

Phytogels are nanostructured hydrogels that incorporate plant-derived bioactive compounds or polymers within the gel matrix [8]. In addition to facilitating targeted and controlled drug release, this design improves the solubility, stability, and bioavailability of phytochemicals, such as flavonoids, alkaloids, and terpenoids [9, 10], while enabling controlled and targeted drug release. Phytogels are typically formed through physical or chemical cross-linking, which imparts strong water absorption and swelling capacity, and maintains stability under physiological conditions [11]. The swelling is predominantly caused by hydrophilic functional groups such as hydroxyl, amide, and sulfonic acid found in the polymer backbone [12] and by combining the therapeutic benefits of natural plants with nanotechnology, phytogels serve as versatile platforms for enhanced drug delivery, tissue engineering, and cosmeceutical applications [13].

Herbal silver nanoparticles (AgNPs) or nanocarriers are generally prepared using plant extracts rather than toxic chemical reducing agents. This environmentally friendly "green synthesis" process reduces silver ions (Ag^+) to nanoparticles through phytochemicals such as flavonoids, phenols, tannins, and terpenoids [14]. Several studies have reported that plant-extract-derived silver nanoparticles exhibit potent antibacterial and antifungal activities, with applications in water purification [9, 10], food packaging [15], wound dressing [16, 17], topical preparations [18], and dental materials [19, 20]. Based on these findings, *F. virens* extract-derived

silver nanoparticles were incorporated into a phytogel formulation and evaluated for their antimicrobial activity.

MATERIALS AND METHODS

Reagents

Silver nitrate (Qulaikems Lifesciences Pvt. Ltd., Vadodara, Gujarat, India), nutrient agar (Rankem), Carbopol 940 (Rankem), triethanolamine (Rankem), polyethylene glycol 400 (Rankem), methyl paraben (Rankem), and other analytical grade reagents were used. Deionized water was employed as the solvent in all experimental procedures.

Extraction of hydroalcoholic extract from *F. virens* bark

The fresh bark of *F. virens* was collected from Kurukshetra University, Haryana, India (29°58′11″ N, 76°52′42″ E). The plant material was authenticated by Dr. Sunita Garg, former Chief Scientist, at RHMD, CSIR-NIScPR, New Delhi, under the Authentication number NIScPR/RHMD/Consult/2021/3972-73-1. The collected bark was thoroughly cleaned, shade-dried at room temperature, and pulverized into a coarse powder. A hydroalcoholic extract (70:30% v/v) was prepared by refluxing 500 g of powdered bark in a Soxhlet apparatus. The extract was concentrated under decreased pressure at 30-45 °C employing a rotary evaporator and stored at 4 °C until further use [21, 22].

Green synthesis of silver nanoparticles using *F. virens* bark extract (*FV-BE*)

AgNPs were synthesized using a green method employing *FV-BE* as a natural stabilizing, capping, and reducing agent. 1 mmol silver nitrate solution (90 ml) was combined with 10 ml of the extract and stirred at 50–60 °C to achieve a volume ratio of 1:9. This produced a brown color, indicating the formation of nanoparticles. After stirring for 12 h in the dark under ambient conditions, the nanoparticles were collected by centrifugation, washed, and redispersed. The yield of AgNPs was calculated based on the theoretical Ag content present in the precursor solution [23]. UV-visible spectroscopy confirmed the synthesis, whereas X-ray diffraction (XRD) and Fourier-transform infrared (FTIR) supported the crystalline structure and the presence of plant-derived functional groups responsible for capping [24, 25].

The percentage yield was then calculated by using the following equation:

$$\text{Yield (\%)} = \text{actual weight of dried AgNPs obtained (mg)} / \text{theoretical silver content from } AgNO_3 \times 100$$

Preformulation studies

Drug-excipient interaction study

FTIR spectroscopy was conducted on the pure components and their physical mixtures to evaluate the compatibility of *FV-BE* with key excipients (Carbopol 940 and triethanolamine). The analysis focused on identifying any notable changes, such as shifts in characteristic peaks or the appearance of new absorption bands, which could indicate physicochemical interactions potentially affecting the stability and effectiveness of the formulation [26]. Following established protocols from the literature, such as *Chadha and Bhandari's* review, highlights the utility of FTIR in compatibility screening [27], *Rojek et al.* combined the FTIR-TG (thermogravimetry) chemometric approach [28], and *Aminu et al.,* applications in ternary systems analysis focused on detecting shifts in characteristic peaks or the emergence of novel bands indicative of physicochemical interactions [29].

Calibration curve development for FV-BE quantification

To prepare the *FV-BE* stock solution, 10 mg of the bark extract was dissolved in 10 ml of phosphate-buffered saline (PBS, pH 7.4). To create serial dilutions from 50 to 500 µg/ml, aliquots (0.5-5.0 ml) of the stock solution were transferred into separate 10 ml volumetric flasks and filled to the mark with PBS (pH 7.4). The absorbance of the dilutions was measured at 274 nm using a UV-visible spectrophotometer. The results were used to create a calibration curve for the quantification of *FV-BE* in subsequent experiments [30-32].

Formulation studies

The gel was prepared using a simple stirring method. Carbopol 940 was dispersed in warm distilled water at concentrations of 0.5, 0.75, and 1% w/w, stirred for 30 min, and allowed to hydrate overnight [33, 34]. AgNPs loaded with *FV-BE* (0.01%–0.03% w/w) were then added, and the pH was adjusted to 6.5–7.0 using triethanolamine to form the gel. PEG 400 and methylparaben were incorporated as the humectant and preservative, respectively [35]. The mixture was homogenized to create a clear, uniform gel. The volume was then adjusted to 100 g using distilled water, and the mixture was stored in airtight containers for further use [36].

Optimization of phytogel formulations using central composite design (CCD)

Phytogel formulations were optimized using CCD via Design-Expert 13.0.5.0, assessing the Carbopol 940 concentration (factor A) and AgNPs with *FV-BE* percentage (factor B) at three levels across 13 runs. Their effects on viscosity, entrapment efficiency, and drug content were analyzed using ANOVA and response surface methodology (RSM). Polynomial regression models described the relationships between variables and responses, supported by R^2 and lack-of-fit tests. Response surface and perturbation plots were used to visualize factor interactions, while the desirability function identified optimal concentrations to achieve suitable viscosity, maximum entrapment efficiency, and drug content [37, 38]. Table 1 shows the levels and ranges of the independent variables used in the phytogel formulation study. Table 2 summarizes the independent variables and the corresponding dependent variables for the phytogel formulations.

Table 1: Process parameters and their ranges

Coded factor	Parameter name	Unit	Low (-1)	Medium (0)	High (+1)
A	Carbopol 940 concentration	% w/w	0.5	0.75	1.0
B	AgNPs+Plant Extract concentration	% w/w	0.01	0.02	0.03

Table 2: CCD experimental runs and observed responses

Run	Carbopol 940 (% w/w)	AgNPs-plant extract (% w/w)	Y1 Viscosity (cps)	Y2 Entrapment efficiency (%)	Y3 Drug content (%)
1	0.75	0.02	5512	91.32	80.65
2	0.50	0.02	4158	78.56	88.25
3	1.00	0.03	7152	81.25	84.25
4	0.75	0.03	5810	88.95	81.95
5	0.50	0.03	4358	76.12	86.95
6	0.75	0.02	5526	90.27	77.65
7	0.75	0.02	5517	91.56	80.25
8	0.75	0.01	5521	89.96	76.95
9	0.50	0.01	4201	75.13	82.98
10	0.75	0.02	5513	93.12	84.21
11	0.75	0.02	5545	91.32	84.56
12	1.00	0.02	6789	85.42	90.23
13	1.00	0.01	6702	82.98	89.98

In vitro evaluation of prepared phytogels

The prepared phytogel formulations were subjected to a series of physicochemical and pharmaceutical tests to assess their suitability for topical application. To ensure quality and stability, each formulation was examined for appearance, homogeneity, clarity, pH, viscosity, extrudability, drug content, entrapment efficiency, *in vitro* drug release, and spreadability [39].

Clarity, appearance, and homogeneity

Each phytogel formulation was visually inspected under ambient light against white and black backgrounds to evaluate the color, transparency, and uniformity. The gels displayed a color range from light brown to dark brown with a translucent appearance and were free from visible lumps or phase separation. The homogeneous texture upon spreading indicates good physical acceptability for topical use [40].

pH determination

The pH of each gel formulation was measured in triplicate using a calibrated digital pH meter after dissolving 1 g of the gel in 100 ml of distilled water and equilibrating at room temperature for 2 h. The mean values were evaluated to demonstrate compatibility with the normal skin pH (4.5-6.5) [41].

Viscosity

To measure viscosity, a Brookfield viscometer (Model DV-II+Pro) with spindle S64 was used at 100 rpm at 25 °C. The spindle was immersed in the sample for 1 min before recording. The viscosity values correlated with the Carbopol 940 concentration, reflecting the gel network density and consistency [42].

Spreadability

Spreadability was tested using the 'drag and slip' method, which involved inserting 1 g of gel between two glass slides and applying a 20 g weight on the upper slide. Spreadability (S) was computed by multiplying the weight (g) and slide length (cm) by the time (T) it required for the slides to separate, with higher S values indicating better spreadability [43].

Extrudability

Approximately 15 g of gel was filled into sealed aluminium tubes and extruded by applying a 500 g load between glass slides. The weight of the extruded gel was calculated as a percentage of the original weight. The formulations were graded as outstanding (>90%), acceptable (>80%), or fair (>70%) based on their extrudability [44].

Drug content

One g of gel was diluted in 100 ml of distilled water and sonicated for three hours to ensure complete drug extraction. The solution was then filtered (0.45 µm), diluted, and examined at 274 nm using UV-visible spectrophotometry. Drug content was estimated using a standard calibration curve [43].

Entrapment efficiency (EE)

EE was calculated indirectly by centrifuging the gel samples at 14,000 rpm for 30 min to remove the unentrapped drug. The free drug in the supernatant was measured at 274 nm, and the EE (%) was calculated as follows:

$$EE\ (\%) = [(W\text{initial drug} - W\text{free drug})/W\text{initial drug}] \times 100.$$

Winitial drug is the amount initially loaded, and Wfree drug is the unentrapped drug measured [45].

Dynamic light scattering (DLS)

DLS was used to examine the particle size distribution and homogeneity of the optimized gels. The samples were diluted with distilled water and analyzed at room temperature using a laser-equipped DLS device with a scattering angle of 90°. The mean hydrodynamic diameter and PDI were determined in triplicate [46].

Zeta potential measurement

The colloidal stability of the optimized phytogel was evaluated by measuring its zeta potential using a Malvern Zeta Sizer at room temperature. The samples were suitably diluted, and measurements were performed in triplicate to ensure reproducibility [46].

Field emission electron microscopy (FESEM)

The surface morphology and microstructure of the lyophilized optimized gel formulation (F7) were investigated using a field-emission scanning electron microscope (JEOL, JSM-7610F plus, Japan). For sample preparation, thin layers of lyophilized phytogels were directly mounted on aluminum stubs using double-sided carbon tape and sputter-coated with a thin gold layer (10 nm) under high vacuum at an accelerating voltage of 5-10 kV. Images were captured at multiple magnifications to observe the morphological features, surface texture, and microstructural arrangements of lyophilized phytogel formations [47].

In vitro drug release

Drug release was examined using a Franz diffusion cell fitted with a dialysis membrane (Molecular weight 12,000-14,000 Da) that was soaked overnight in PBS (pH 7.4) and had an effective diffusion area of 2 cm^2 [48]. One g of gel was placed in the donor compartment, while the receptor chamber contained PBS (pH 7.4), maintained at 37±0.5 °C, and swirled at 100 rpm [49]. To maintain sink conditions, 1 ml aliquots were taken at regular intervals and replenished with new buffer. Drug concentration was determined spectrophotometrically at 274 nm [50].

Release kinetics

The cumulative drug release data were fitted to different kinetic models, including zero-order, first-order, Higuchi, and Korsmeyer-Peppas models, to determine the release mechanism and kinetics of the gel [51]. The zero-order model was expressed as $C_t = C_0 + K_0 t$, where Ct is the drug concentration at time t, C_0 is the initial concentration, and K_0 is the zero-order release constant. The first-order model is represented as $\log C = \log C_0 - (Kt/2.303)$, where C is the concentration of the drug remaining at time t, C_0 is the initial concentration, and Kt is the first-order release rate constant ($time^{-1}$). The Higuchi model is given by $Q_t = K_H . t_{1/2}$, where Qt is the cumulative drug released at a given time per unit area, $t_{1/2}$, and KH is the Higuchi dissolution constant. The Korsmeyer-Peppas model was expressed as $\log (Mt/M\infty) = \log Kkp + n \log t$, where M_t is the amount of drug released at time t, $M\infty$ is the cumulative amount of drug released at infinite time, Kkp is the release rate constant, and n is the release exponent [52].

Stability studies

The stability evaluation followed the ICH Q1A guidelines. The optimized gel was stored in sealed containers under refrigerated (4±2 °C), room temperature (25±2 °C), and accelerated (40±2 °C, 75±5% RH) conditions for three months. Assessments at 30, 60, and 90 days included physical appearance, pH, particle size, drug content, spreadability, entrapment efficiency, and viscosity to monitor the formulation integrity over time [53].

In vitro biological evaluation

Antimicrobial activity

The antimicrobial potential of the phytogel formulations was assessed against *E. coli (MTCC 443)*, *S. aureus (MTCC 96)*, *P. aeruginosa (MTCC 1688)*, and *A. niger (MTCC 282)* by using the agar well diffusion method. Sterile nutrient agar plates (for bacteria) and Sabouraud dextrose agar plates (for fungi) were uniformly inoculated with the respective microbial suspensions. Wells of 6 mm diameter were aseptically prepared and filled with 100 µl** of the test formulations. The inoculated plates were incubated at 37 °C for 24 h for bacterial strains, whereas *A. niger* plates were incubated at 28±2 °C for 48-72 h to ensure optimum fungal growth and metabolite diffusion. A commercial Ag nanogel containing 0.002% nanocrystalline Ag was used as the reference control. Since the F7 formulation contained 0.02% AgNPs (ten-fold higher), antimicrobial activity data were normalized to equivalent silver concentrations to allow valid comparison. After normalization, the diameters of inhibition zones (mm) were measured and expressed as

mean±SD of triplicate experiments. The data were statistically analyzed using one-way ANOVA followed by Tukey's post-hoc test, with $p < 0.05$ considered significant [54, 55].

RESULTS

Yield of silver nanoparticles

The theoretical silver content in 90 ml of 1 mmol $AgNO_3$ was calculated as 9.71 mg. After centrifugation, repeated washing, and drying, the actual mass of AgNPs recovered was 6.89 mg, corresponding to a percentage yield of 70.9%.

Pre-formulation studies

Drug-excipient interaction study via FTIR

FTIR analysis was performed to evaluate the possible interaction between *FV-BE* and the formulation excipients. The spectrum of *FV-BE* (fig. 1) displayed characteristic bands: a broad band at 3600–3200 cm^{-1} due to O–H and N–H stretching, peaks at 2920–2850 cm^{-1} from aliphatic C–H stretching, a strong absorption near 1715 cm^{-1} corresponding to C=O stretching, and a band at ~1620 cm^{-1} attributed to C=C stretching of the aromatic and alkene groups. Additional peaks at ~1375 cm^{-1} (C–H bending), ~1020 cm^{-1} (C–O stretching), and minor signals below 900 cm^{-1} confirmed the presence of polyphenolic and carbohydrate components.

The comparative FTIR spectra of *FV-BE* and its physical mixture with excipients showed no significant shifts, losses, or appearance of new absorption bands. The key functional groups of *FV-BE* remained intact, whereas minor overlaps were attributable to spectral superimposition. These results confirmed the absence of chemical interactions, demonstrating the excellent compatibility of *FV-BE* with the excipients and supporting the stability of the formulation.

X-ray diffraction (XRD)

The XRD pattern of the biosynthesized silver nanoparticles (AgNPs) derived from *FV-BE* is shown in fig. 2. The diffraction peaks at 2θ values of 38.1°, 44.3°, 64.5°, and 77.4° correspond to the (111), (200), (220), and (311) crystallographic planes of face-centered cubic (fcc) metallic silver, respectively. These characteristic peaks confirmed the crystalline nature and high purity of the synthesized silver nanoparticles. The sharpness and strength of these peaks further suggest good crystallinity. The optimized phytogel formulation (F7) displays a relatively flattened XRD pattern with no prominent peaks related to silver, indicating the absence of crystalline silver nanoparticles in their free form or a possible dispersion of AgNPs within the gel matrix. This indicated successful incorporation and compatibility of the nanoparticles in the gel system without significant changes to their crystalline structure. The observed peaks align well with standard JCPDS data for metallic silver, confirming the reduction of silver ions to elemental silver nanoparticles through the plant extract. This validates the effectiveness of the biological synthesis method in producing crystalline AgNPs suitable for incorporation into the phytogel. In the XRD graph provided, the optimized gel formulation (labeled "F7 optimized gel formulation" in red) shows a prominent peak around 44° 2θ. No other significant sharp peaks are clearly visible for the gel formulation; the rest of the pattern appears more like a broad background or amorphous halo typical of gel or polymer matrices. This suggests that the gel formulation primarily exhibits an amorphous or less crystalline nature, possibly with a peak overlapping the (111) plane of AgNPs (around 44°) from the AgNPs spectrum.

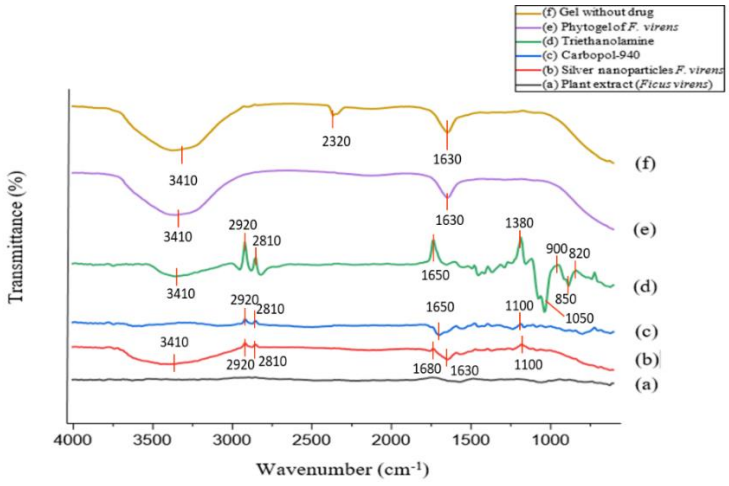

Fig. 1: FTIR spectra of *FV-BE*, AgNPs, phytogel formulation, and excipients

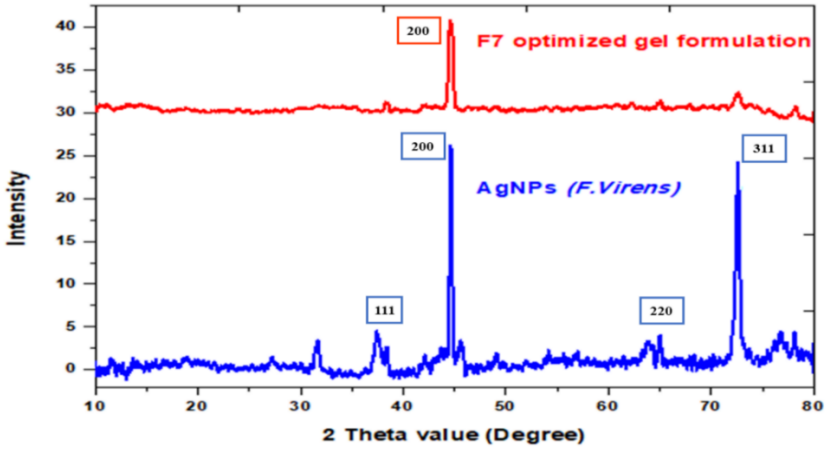

Fig. 2: Overlay XRD spectra of AgNPs (*F. virens*) and optimized gel formulation (F7)

Calibration curve of *FV-BE*

A calibration curve for *FV-BE* was established by measuring absorbance at 274 nm in phosphate buffer (pH 7.4) across a range of concentrations. Linear regression analysis produced the equation Y = 0.1062x+0.0053 (R^2 = 0.9907), indicating a strong linear correlation suitable for the accurate quantification of *FV-BE* in formulation studies (fig. 3).

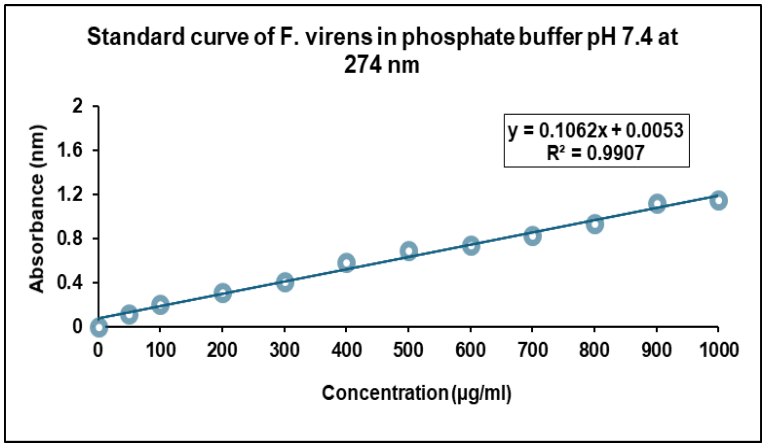

Fig. 3: Standard calibration curve of *FV-BE in* phosphate buffer (pH 7.4)

Formulation, optimization using central composite design (CCD)

CCD was employed to optimize *F. virens* phytogel formulations, examining the effects of Carbopol 940 concentration (A) and combined silver AgNPs with *FV-BE concentration* (B) on key responses: viscosity (Y_1), entrapment efficiency (Y_2), and drug content (Y_3). Thirteen formulations with varying A and B levels were prepared and analyzed in triplicate. Polynomial regression models describe the relationships between independent variables and responses as follows (in coded terms):

$$\sqrt{\text{Viscosity}}\ (Y_1) = 74.32+8.92A+0.97B+0.38AB - 0.91A^2+0.92B^2$$

$$\sqrt{\text{Entrapment Efficiency}}\ (Y_2) = 9.58+0.19A - 0.02B - 0.04AB - 0.55A^2 - 0.14B^2$$

$$\sqrt{\text{Drug Content}}\ (Y_3) = 9.03+0.06A+0.03B+0.39A^2 - 0.14B^2$$

These models enabled the accurate prediction of the formulation performance within the tested variable ranges. Carbopol 940 concentration was the dominant factor, exerting a strong positive linear effect on viscosity while also showing nonlinear effects indicated by significant negative quadratic terms. AgNPs combined with plant extract moderately increased viscosity but had minimal impact on entrapment efficiency.

Table 3: ANOVA summary for the quadratic model of square root-transformed viscosity response using coded factor levels

Source	Sum of squares	df	mean square	F-value	p-value	
Model	486.91	5	97.38	16293.57	<0.0001	significant
A-Carbopol 940	477.36	1	477.36	79870.56	<0.0001	
B-AgNPs	5.65	1	5.65	945.78	<0.0001	
AB	0.5653	1	0.5653	94.58	<0.0001	
A^2	2.29	1	2.29	382.56	<0.0001	
B^2	2.31	1	2.31	386.52	<0.0001	
Residual	0.0418	7	0.0060			
Lack of Fit	0.0080	3	0.0027	0.3132	0.8163	not significant
Pure Error	0.0339	4	0.0085			
Cor Total	486.95	12				

Note: P-values<0.05, significant effects; values ≥0.05, non-significant effects.

Table 4: ANOVA summary for the quadratic model of square root-transformed entrapment efficiency response using coded factor levels

Source	Sum of squares	df	mean square	F-value	p-value	
Model	1.42	5	0.2848	134.08	<0.0001	significant
A-Carbopol 940	0.2052	1	0.2052	96.62	<0.0001	
B-AgNPs	0.0014	1	0.0014	0.6631	0.4423	
AB	0.0058	1	0.0058	2.73	0.1423	
A^2	0.8209	1	0.8209	386.50	<0.0001	
B^2	0.0541	1	0.0541	25.49	0.0015	
Residual	0.0149	7	0.0021			
Lack of Fit	0.0034	3	0.0011	0.3976	0.7627	not significant
Pure Error	0.0115	4	0.0029			
Cor Total	1.44	12				

Note: P-values<0.05, significant effects; values ≥0.05, non-significant effects.

Table 5: ANOVA summary for the quadratic model of square root-transformed drug content response using coded factor levels

Source	Sum of squares	df	mean square	F-value	P-value	
Model	0.5200	5	0.1040	5.13	0.0270	significant
A-Carbopol 940	0.0187	1	0.0187	0.9243	0.3684	
B-AgNPs	0.0059	1	0.0059	0.2932	0.6050	
AB	0.0682	1	0.0682	3.36	0.1093	
A^2	0.4269	1	0.4269	21.05	0.0025	
B^2	0.0549	1	0.0549	2.71	0.1438	
Residual	0.1419	7	0.0203			
Lack of Fit	0.0380	3	0.0127	0.4873	0.7094	not significant
Pure Error	0.1039	4	0.0260			
Cor Total	0.6620	12				

Note: P-values<0.05, significant effects; values ≥0.05, non-significant effects.

Table 6: Regression coefficients and p-values for quadratic models of square root-transformed viscosity, entrapment efficiency, and drug content responses coded factors

Responses	Intercept	A	B	AB	A^2	B^2
Sqrt (viscosity)	74.3241	8.91963	0.970618	0.375932	-0.909859	0.914563
p-values		<0.0001	<0.0001	<0.0001	<0.0001	<0.0001
Sqrt (Entrapment efficiency)	9.57543	0.184944	-0.0153217	-0.0380947	-0.545194	-0.140017
p-values		<0.0001	0.4423	0.1423	<0.0001	0.0015
Sqrt (% Drug content)	9.03282	0.0558874	0.0314788	-0.13059	0.393147	-0.14103
p-values		0.3684	0.6050	0.1093	0.0025	0.1438

Note: P-values<0.05, significant effects; values ≥0.05, non-significant effects.

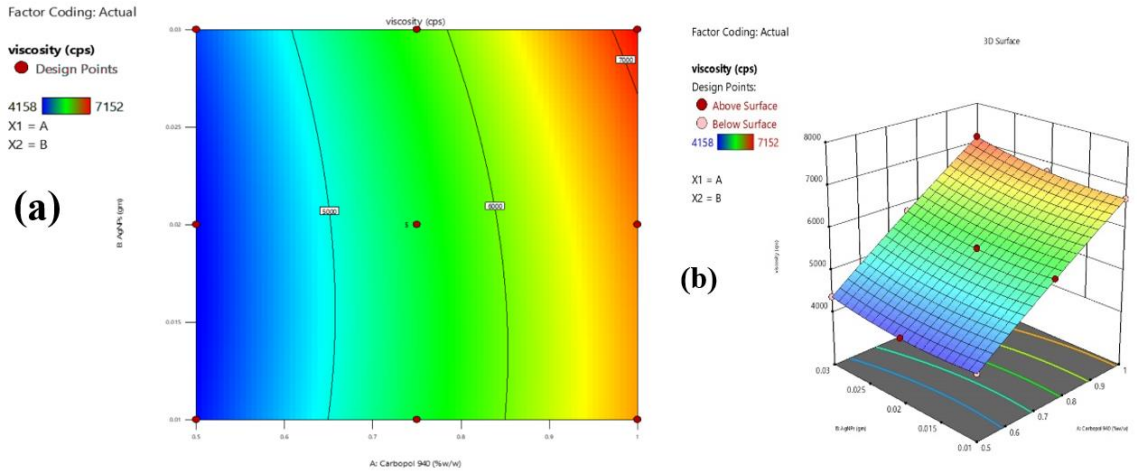

Fig. 4: Contour (a) and 3D response surface (b) plots illustrating the effects of carbopol 940 and combined AgNPs with *FV-BE concentrations* on phytogel viscosity

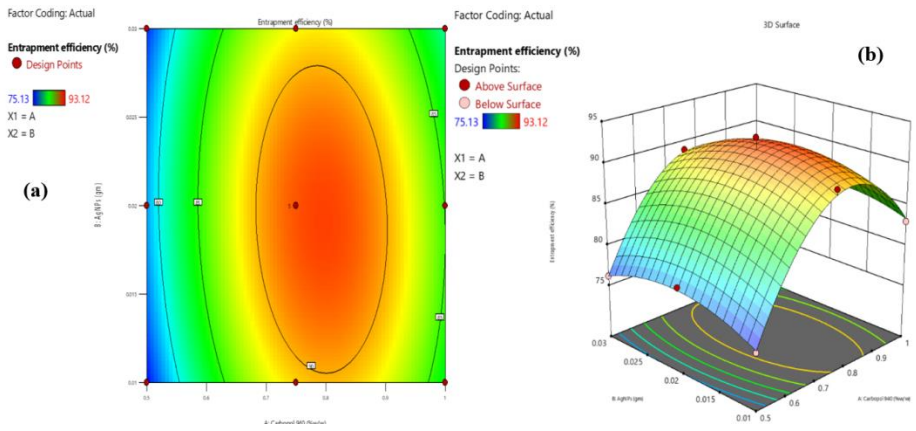

Fig. 5: Contour (a) and 3D response surface (b) plots showing the effects of Carbopol 940 and combined AgNPs with *FV-BE* concentrations on entrapment efficiency

Effect of independent variables on viscosity

The viscosity of the phytogel formulation increased significantly with increasing concentrations of Carbopol 940. The incorporation of AgNPs into *FV-BE produced* a moderate increase in viscosity. A mild synergistic effect was observed at higher concentrations, leading to further viscosity enhancement. This trend is advantageous for optimizing formulations to achieve the desirable gel consistency and effective spreadability, as shown in fig. 4(a) and (b).

Effect of independent variables on entrapment efficiency

The EE of the AgNPs-loaded phytogel was mainly affected by the concentration of Carbopol 940, which improved drug encapsulation by forming a denser gel network. However, beyond the optimal level, excessive Carbopol 940 reduced EE, likely due to the increased viscosity-limiting drug distribution. The combination of AgNPs and *FV-BE* had a minimal, slightly negative effect at higher concentrations, possibly because of particle aggregation. Interaction effects were minor but noticeable at elevated levels. These findings emphasize the importance of optimizing the polymer content while carefully managing the nanoparticle load to achieve maximum entrapment efficiency (fig. 5a and 5b).

Effect of independent variables on drug content

The drug content in the AgNPs-loaded phytogel was mainly driven by the Carbopol 940 concentration, with higher polymer levels enhancing drug retention through a stronger and denser gel matrix. This effect was nonlinear, showing a marked increase in drug content as carbopol 940 concentration increased. AgNPs combined with *FV-BE also* positively influenced drug content by providing additional binding sites, although excessive AgNPs levels led to a decline, likely due to agglomeration or saturation limiting drug incorporation. These findings highlight carbopol 940 as the primary factor in drug loading, with the nanoparticle concentration serving as a secondary regulator, emphasizing the need for balanced optimization (fig. 6a and 5b).

.

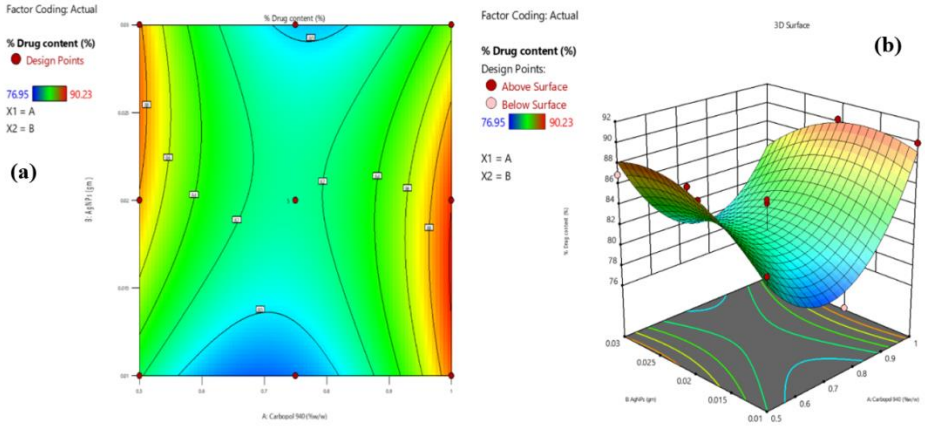

Fig. 6: Contour (a) and 3D response surface (b) plots depicting the effects of carbopol 940 and AgNPs with *FV-BE* on drug content

Desirability-based optimization and selection of AgNPs-loaded phytogel

Contour plots of the desirability function were used to guide the multi-response optimization of the AgNPs-loaded phytogel, simultaneously maximizing viscosity, entrapment efficiency, and drug content. The optimal formulation was achieved with intermediate to high concentrations of Carbopol 940 and moderate levels of AgNPs combined with *FV-BE*, ensuring balanced application, stability, and effective drug encapsulation (fig. 7).

The optimized formulation F7 (0.75% w/w Carbopol 940 and 0.02% w/w AgNPs with *FV-BE*) was identified as the most desirable candidate based on response surface modeling. The predicted and experimental values for viscosity, entrapment efficiency, and drug content closely matched, confirming the accuracy of the model. F7 showed a good balance between high drug loading, excellent entrapment efficiency, and appropriate viscosity. The formulation exhibited superior extrudability and spreadability, enhance patient acceptability, and rheological analysis confirmed non-Newtonian shear-thinning behavior, facilitating easy application and diffusion-controlled release at the site.

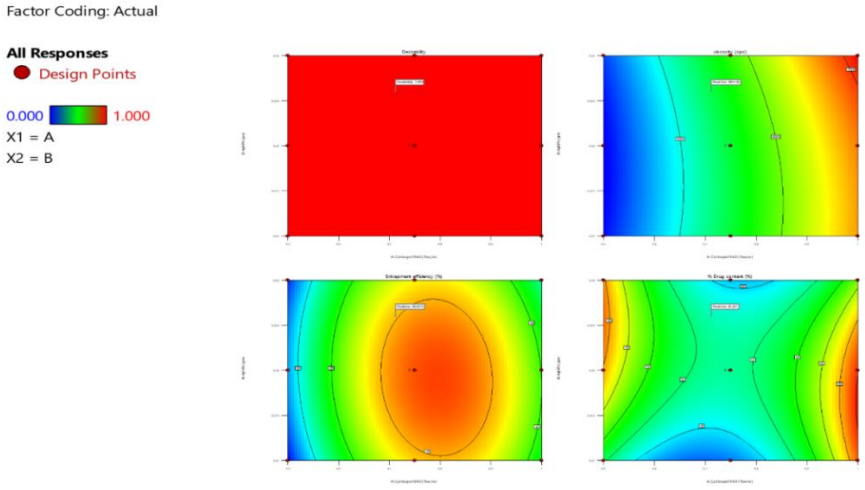

Fig. 7: Contour plots of desirability index for multi-response formulation optimization on viscosity, entrapment efficiency, and drug content

Table 7: Predicted and observed values of viscosity, entrapment efficiency, and % drug content for optimized formulation (F7), expressed as mean±SD

Analysis	Predicted mean	Observed mean (F7)
Viscosity	5522.05 ±23.9	5517 ±7.07
Entrapment efficiency	91.594±1.082	91.56±0.131
% Drug content	81.7635±2.501	80.25±1.3621

Value are expressed as mean±SD (n=3)

Table 7 presents the predicted responses at varying factor levels with confidence and tolerance intervals, supporting robust optimization and model validation. Predicted values were obtained from the response surface quadratic model, while observed values correspond to the experimental results of the optimized formulation (F7).

Table 8: Formulation table of *F. virens* AgNPs loaded phytogel

Ingredients	F1	F2	F3	F4	F5	F6	F7	F8	F9	F10	F11	F12	F13
Carbopol 940 (%w/w)	0.75	0.5	1.0	0.75	0.50	0.75	0.75	0.75	0.5	0.75	0.75	1.0	1.0
AgNPs+Plant extract (% w/w)	0.02	0.02	0.03	0.03	0.03	0.02	0.02	0.01	0.01	0.02	0.02	0.02	0.01
Triethanolamine (ml)	1.0	1.0	1.0	1.0	1.0	1.0	1.0	1.0	1.0	1.0	1.0	1.0	1.0
Methyl Paraben (gm)	0.08	0.08	0.08	0.08	0.08	0.08	0.08	0.08	0.08	0.08	0.08	0.08	0.08
Polyethylene Glycol (PEG 400) (ml)	0.2	0.2	0.2	0.2	0.2	0.2	0.2	0.2	0.2	0.2	0.2	0.2	0.2
Distilled water (ml)	Q. S.	Q. S.	Q. S.	Q. S.	Q. S.	Q. S.	Q. S.	Q. S.	Q. S.	Q. S.	Q. S.	Q. S.	Q. S.

***In vitro* evaluation of the parameters of prepared phytogels**

Physicochemical evaluation of phytogel formulations (F1–F13)

The prepared phytogel formulations were evaluated for key physicochemical properties relevant to topical application and patient acceptability.

Color, appearance, and homogeneity

The control gel with plain Carbopol 940 was translucent and colorless, whereas all AgNPs-loaded phytogels exhibited a uniform brownish-yellow color attributed to the AgNPs and *FV-BE*. All the formulations were free of lumps and foreign particles, demonstrating excellent homogeneity.

pH determination

Formulation pH values ranged from 6.22±0.09 to 6.95±0.03, remaining near neutral and within skin-compatible limits, thereby minimizing the potential for irritation (table 9).

Viscosity

Viscosity increased with Carbopol 940 concentration, ranging from 4201±1.7 cps to 7152±0.8 cps (F1-F13). Formulation F3 (1.5% Carbopol 940) showed significantly higher viscosity than F9 (0.5% Carbopol 940), aligned with the values of marketed topical gels. Elevated viscosity supports prolonged skin residence and has a potential therapeutic efficacy (table 9).

Spreadability

Spreadability, assessed by spreading time, varied between 15.3 and 53 seconds. Lower viscosity formulations spread more rapidly, while higher viscosity gels showed slower spread, indicating an appropriate balance for uniform topical application comparable to commercial products (table 9).

Extrudability

All gels exhibited high extrudability (>80%), with some formulations exceeding 90%, facilitating easy dispensing from the collapsible tubes. For example, F7 demonstrated superior extrudability relative to F9, which is consistent with marketed standards. Rheological profiles confirmed shear-thinning behavior, which is beneficial for ease of application and retention on the skin (table 10).

Drug content (%)

The drug content ranged from 76.95±0.62% to 92.95±1.12% across formulations, with F7 showing the highest drug loading. Uniform drug distribution within all gels reflected consistent formulation reproducibility (table 9).

Table 9: Results of drug content, appearance, pH, spreadability, viscosities, and entrapment efficiency tests of all formulations

Formulation code	Drug content (%)	Appearance	pH	Viscosity at 100 rpm (cps)	Spreadability (g. cm/s)	Entrapment efficiency (%)
F1	80.65±0.66	Light brown	6.40±0.009	5512±2.2	11.49±1.18	80.65±0.25
F2	88.25±0.27	Brown	6.48±0.008	4158±1.7	11.07±1.03	88.25±0.33
F3	84.25±0.55	Dark brown	6.53±0.008	7152±0.8	14.46±1.72	84.25±0.14
F4	81.95±0.42	Light brown	6.53±0.017	5810±1.7	18.30±1.28	81.95±0.87
F5	86.25±1.08	Brown	6.62±0.083	4358±0.8	19.39±0.21	86.95±0.24
F6	77.65±1.21	Dark brown	6.22±0.087	5526±1.2	17.90±1.63	77.65±0.47
F7	92.95±1.12	Light brown	6.64±0.097	5517±1.2	12.75±1.67	90.23±0.37
F8	76.95±0.62	Brown	6.86±0.045	5521±0.5	11.64±1.44	76.95±0.89
F9	82.98±1.0	Dark brown	6.72±0.008	4201±1.7	11.60±1.24	82.98±0.29
F10	84.21±2.5	Light brown	6.54±0.077	5513±0.9	17.90±1.63	84.21± 0.56
F11	84.56±1.2	Light brown	6.74±0.019	5545±1.2	17.90±1.63	84.56±0.44
F12	89.23 ±1.8	Dark brown	6.95±0.027	6789 ±0.9	17.90±1.63	80.25±0.51
F13	89.98±0.41	Light brown	6.64±0.016	6702 ±0.7	17.90±1.63	89.98±0.84

Note: All values are means of triplicate values (n=3)±SD

Table 10: Extrudability profile of gel formulations

Formulation code	Weight of formulation (g)	Weight of gel extruded (g)	Extrudability amount (%)	Grade
F1	15.91	13.65	85.79	Good
F2	15.48	13.25	85.59	Good
F3	15.25	13.42	88.00	Good
F4	15.02	13.48	89.75	Good
F5	15.41	14.21	90.21	Excellent
F6	15.89	13.65	85.90	Good
F7	14.95	13.58	90.83	Excellent
F8	15.67	13.15	83.92	Good
F9	15.95	12.57	78.81	Fair
F10	15.21	13.54	89.02	Good
F11	15.26	13.24	86.76	Good
F12	15.17	12.98	85.56	Good
F13	14.93	13.51	90.49	Excellent

Entrapment efficiency (EE)

EE across formulations F1-F13 ranged from 76.95±0.89% to 90.23±0.37%, with F7 achieving the highest EE. A positive correlation was observed between Carbopol 940 concentration and EE, indicating that increased polymer content enhances drug encapsulation within the gel matrix (table 9).

Dynamic light scattering (DLS)

DLS analysis of formulation F7 showed an average particle size of 259.5 nm and a PDI of 0.280, indicating moderate particle size uniformity. These data suggest that the concentration of Carbopol 940 plays a role in producing smaller, well-dispersed particles, contributing to gel stability and consistency (fig. 8).

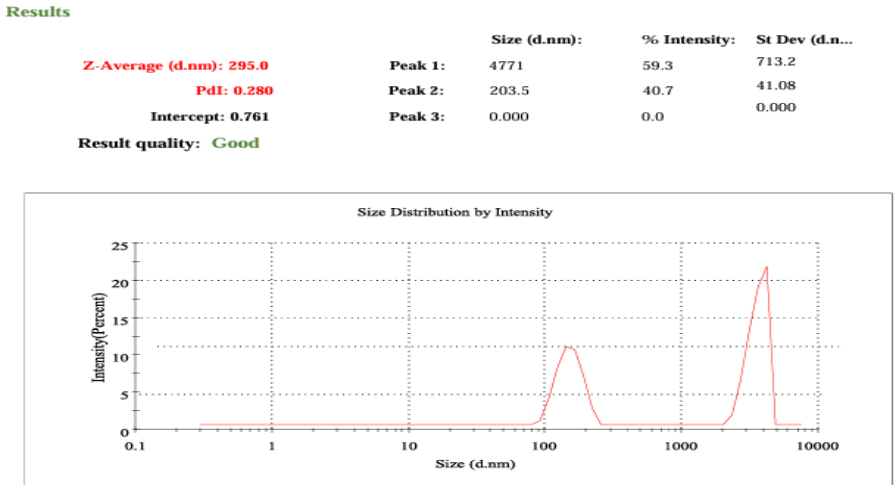

Fig. 8: DLS profile of optimized phytogel

FESEM microscopy

The FESEM micrographs (fig. 9) demonstrated that the lyophilized phytogel exhibited a distinct surface morphology characterized by a rough and porous texture. At 100X magnification, irregular distribution and particulate features were evident across the surface, while at 200X magnification, entrapped nanoparticles could be more clearly observed within the polymeric network. The observed surface morphology confirmed the successful incorporation of nanoparticles into the phytogel matrix, which may contribute to controlled drug release.

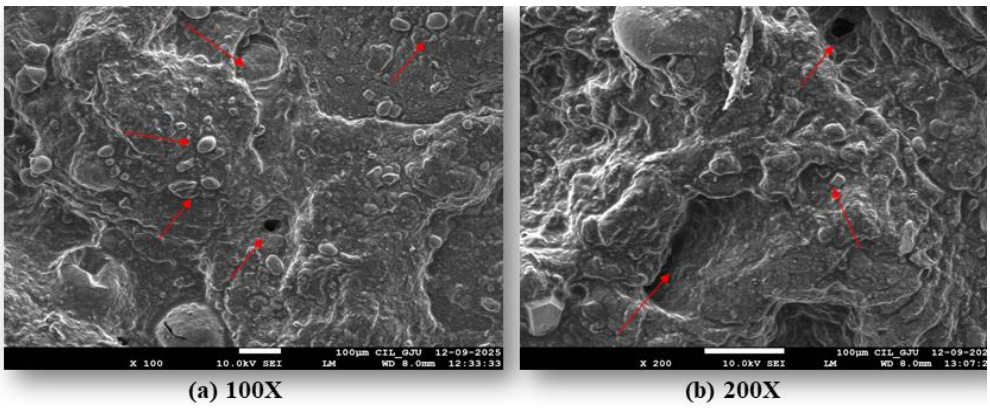

Fig. 9: FESEM micrographs of lyophilized optimized phytogel (F7) at (a) 100X and (b) 200X magnifications (Note: red arrows indicate porous structure, surface irregularities, and embedded particulate structures)

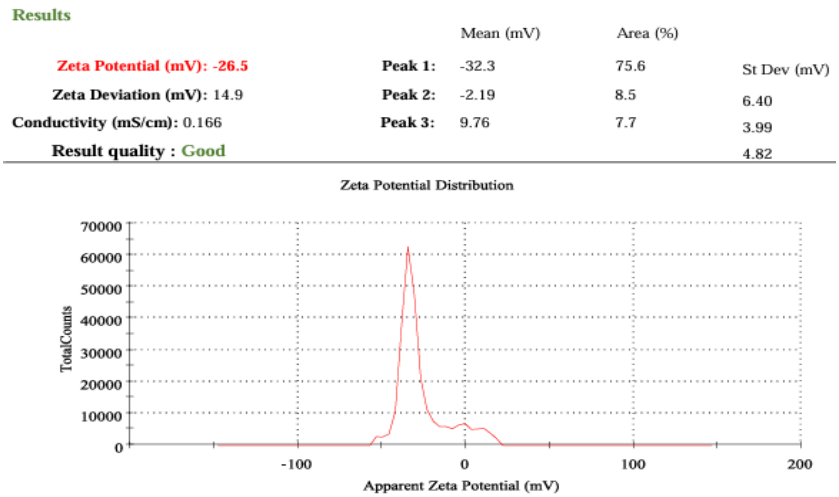

Fig. 10: Zeta potential measurement

Zeta potential

The optimized phytogel (F7) exhibited a zeta potential of −26.5 mV, confirming good colloidal stability through effective electrostatic repulsion. The negative charge arises from the anionic nature of the polymer and drug, which prevents nanoparticle aggregation and maintains a stable dispersion, as illustrated in fig. 10.

In vitro drug release studies

Cumulative drug release over 24 h varied from 58.93% to 98.86%, with F7 exhibiting the highest release (98.86%±0.24%). In contrast, the plain gel base released only 30.62%±0.50%. Formulation F7, containing 0.75% Carbopol 940 and 0.02% AgNPs with *FV-BE*, showed optimal combined parameters, including pH (6.64±0.097), drug content (92.95%±1.12%), viscosity (5517±1.2 cps), and spreadability (12.75±1.67 g. cm/s), extrudability (90.83%), contributing to enhanced drug permeation (table 9, 10). The complete diffusion-controlled release observed across formulations suggests the effective maintenance of therapeutic drug levels (fig. 11). The results underscore the integral role of Carbopol 940 concentration and AgNPs-plant extract combination in modulating the physicochemical and drug release characteristics of the phytogel.

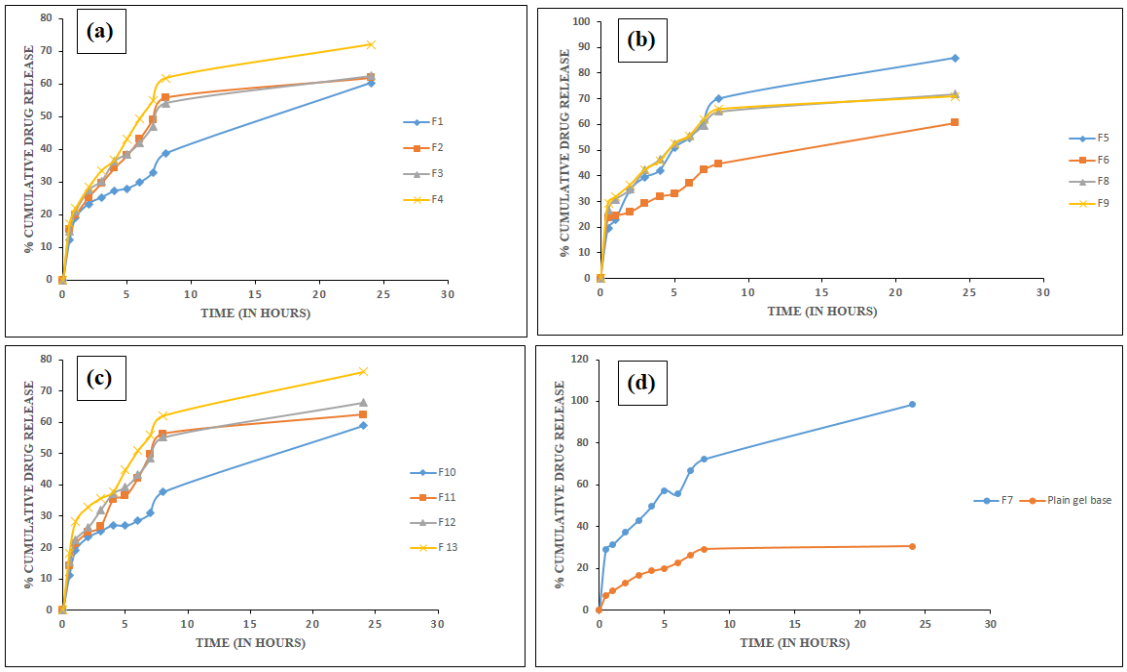

Fig. 11: *In vitro* drug permeation profiles of *FV-BE-loaded* AgNPs gels: (a) formulations F1–F4, (b) F5–F6, F8-F9, (c) F10–F13 (mean±SD, n=3), and (d) comparison between plain drug gel and optimized formulation F7

Drug release kinetics

The *in vitro* drug release profile of the optimized phytogel formulation F7 was analyzed using Zero-order, First-order, Higuchi, and Korsmeyer-Peppas models. Regression analysis revealed that the first-order model best described the release kinetics, with the highest correlation coefficient (R^2 = 0.9864), indicating concentration-dependent release. The Korsmeyer-Peppas model also demonstrated a strong fit (R^2 = 0.9899), suggesting that diffusion is a key mechanism controlling drug release (table 11). The lower R^2 values for the zero-order (0.5896) and Higuchi (0.9789) models further supported these conclusions (fig. 12).

Table 11: Regression coefficients (R^2) for drug release kinetics models of formulation F7

Formulation	Zero-order model	First-order model	Higuchi model	Korsmeyer-peppas model	
	R^2value	R^2value	R^2value	R^2value	n value
F7 (Optimized formulation)	0.5896	0.9864	0.9789	0.9899	0.7907

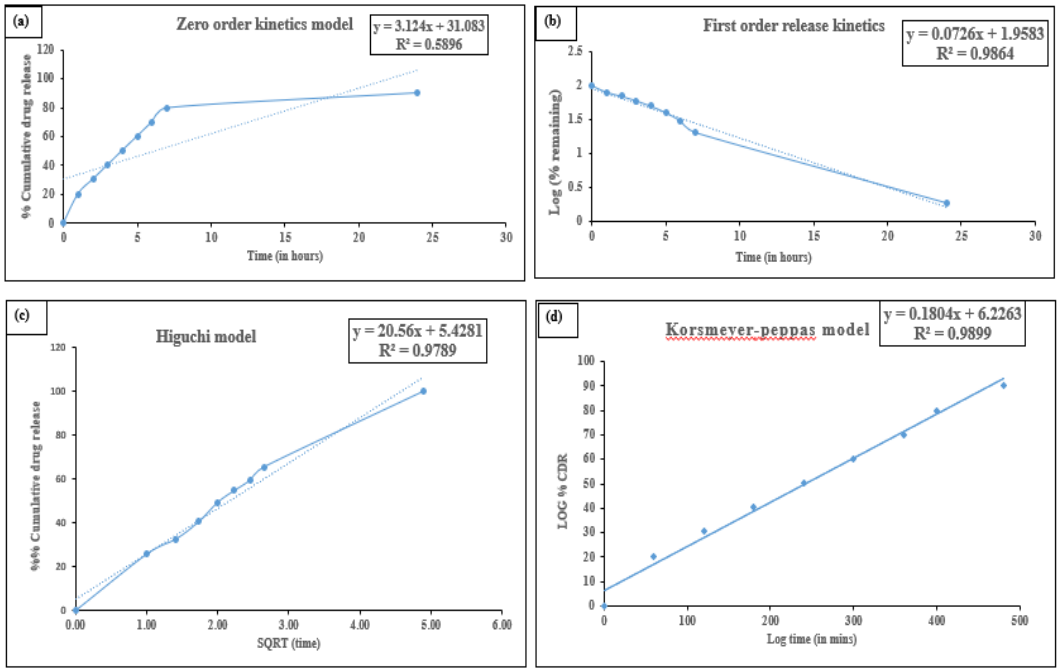

Fig. 12: *In vitro* drug release kinetics of phytogel F7 fitted to (a) Zero-order, (b) First-order, (c) Higuchi, and (d) Korsmeyer-peppas models

The release exponent (n) characterizes the drug transport mechanism from the delivery system. According to table 12, values of 0.5<n<1.0 indicate anomalous (non-Fickian) transport. The obtained n value of 0.7907 confirms that drug release at different pH conditions follows a non-Fickian diffusion mechanism. Anomalous (non-Fickian) transport is possible in a nanogel-based AgNPs platform because the release of AgNPs is dependent on diffusion through the nanogel matrix and polymer swelling or relaxation. This integrated mechanism enables long-term and controllable delivery, which is dependent on the nanogel design and sensitivity to environmental factors that promote antimicrobial bioactivity and targeted distribution [54].

Table 12: Drug transport mechanism for different values of drug release exponent (n)

Release exponent (n)	Drug transport mechanism
n <0.5	Quasi-Fickian diffusion
0.5	Fickian diffusion
0.5 <n < 1.0	Non-Fickian diffusion (Anomalous)
Higher than 1.0	Case II transport

Stability studies

Over three months, formulation F7 remained stable under refrigerated, ambient, and accelerated conditions, preserving its characteristic light brown color. No significant changes were observed in pH, entrapment efficiency, or drug content, confirming the robustness of the formulation and minimal drug degradation under varying storage environments (table 13).

Table 13: Stability study results of *FV-BE-loaded* AgNPs phytogel formulation (F7)

Parameters	F7 (optimized formulation batch)	4±2 °C (Refrigerated)	25±2 °C/60% RH (Ambient)	40±2 °C/75% RH (Accelerated)
Appearance	Light brown	Light brown	Light brown	Light brown
pH	6.64±0.097	6.45±0.71^{ns}	6.31±0.47^{ns}	6.28 ±0.85^{ns}
Viscosity	5517 ±1.2	5548±0.54^{ns}	5526±0.31^{ns}	5499±0.2^{ns}
Entrapment efficiency %	90.23±0.37%	89.58±0.15%^{ns}	88.59±0.27%^{ns}	88.48±0.48%^{ns}
Drug Content	92.95±1.12%	91.5±0.18%^{ns}	91.8±0.27%^{ns}	91.2±0.84%^{ns}
Microbial growth	Absent	Absent	Absent	Absent

Note: value are expressed as mean±SEM (n = 3). Data were analyzed using one-way ANOVA with Tukey's post-hoc test. ^{ns}p>0.05 as compared to the F7 optimized formulation

In vitro antimicrobial activity

The mean inhibition zones of the phytogel formulation were measured after 24h for *E. coli*, *S. aureus*, *P. aeruginosa*, and after 72h for *Aspergillus niger*. The mean inhibition zones of phytogel formulation against *E. coli*, *S. aureus*, *P. aeruginosa*, and *A. niger* were found to be 19.5±0.7, 19.3±0.9, 16.8±0.4, and 15.3±0.6 mm, respectively. The standard drug chloramphenicol exhibited antimicrobial activity against *E. coli* (22±0.4), *S. aureus* (20±0.5), and *P. aeruginosa* (21±0.7), while the standard antifungal ketoconazole showed an inhibition zone of 23±0.9 mm against *A. niger* (table 14).

Statistical analysis (unpaired t-test) revealed a significant difference between the phytogel formulation and the standard for *E. coli* ($p<0.05$), *P. Aeruginosa* ($p<0.01$), and *A. niger* ($p<0.01$), where no significant differences were observed for *S. aureus*. These findings indicate that the phytogel formulation possesses notable antimicrobial efficacy, comparable to that of the standard drugs (fig. 13).

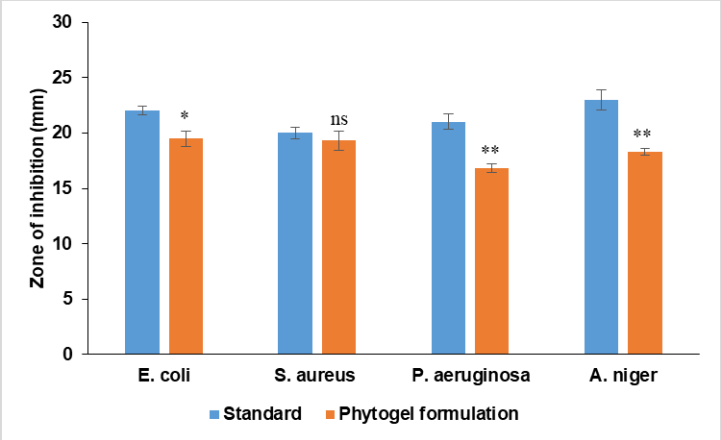

Fig. 13: Antimicrobial action of *FV-BE*-loaded AgNPs phytogel formulation, n=3, the data (mean±SEM) were analyzed using unpaired t-tests, $^{ns}p>0.05$, *p<0.05, **p<0.01, as compared with the respective standard

Table 14: Antimicrobial action of *FV-BE-loaded* AgNPs phytogel formulation

Treatment	*E. coli*	*S. aureus*	*P. aeruginosa*	*A. niger*
Standard	22±0.4	20±0.5	21±0.7	23±0.9
Phytogel formulation	19.5±0.7*	19.3±0.9^{ns}	16.8±0.4**	18.3±0.3**
P-value	(p<0.05)	(p>0.05)	(p<0.01)	(p<0.01)

n=3, the data (mean±SEM) were analyzed using an unpaired t-test, $^{ns}p>0.05$, *p<0.05, **p<0.01, compared with the respective standard

DISCUSSION

The development and optimization of a novel phytogel formulation incorporating silver nanoparticles (AgNPs) and *Ficus virens* bark extract (*FV-BE*) showed promising results for topical antimicrobial use. Systematic evaluation using CCD revealed that the amounts of Carbopol 940 and AgNPs significantly affected the formulation's physicochemical properties and drug release profile. The optimized formulation, F7, containing 0.75% w/w Carbopol 940 and 0.02% w/w AgNPs with *FV-BE*, exhibited desirable characteristics, including suitable viscosity (5517±1.2 cps), spreadability (12.75±1.67 g. cm/s), and pH (6.64±0.097), making it appropriate for topical application. The results align with previous research, which demonstrated that gels made with Carbopol 940 exhibit desirable rheological properties and are compatible with the skin in nanocarrier formulations [56]. The high entrapment efficiency (90.23±0.37%) and drug content (92.95%±1.12%) suggest effective incorporation of active ingredients into the gel. High encapsulation efficiencies, similar to those reported for phytochemical-loaded AgNPs like *Azadirachta indica*-AgNPs gels and curcumin-loaded chitosan nanocarriers, have been documented, with values ranging from 80 to 90% [57, 58]. This suggests that *FV-BE* interacts effectively with the polymer and silver matrix, thereby optimizing drug retention.

Particle size analysis revealed an average size of 259.5 nm with a PDI of 0.280, indicating a relatively uniform nanoparticle distribution. Earlier studies on plant-based AgNPs formulations using *Withania coagulans* have generally reported an average particle size of 174.9±0.062 nm [59]. The zeta potential of-26.5 mV indicates a moderate level of colloidal stability, comparable to values observed in other AgNPs-based topical formulations. Previous reports have shown that stable AgNP suspensions synthesized with herbal extracts typically exhibit zeta potentials ranging from-20 to-30 mV, whereas formulations with a zeta potential of-15 mV tend to aggregate more quickly and have a shorter shelf-life. Consequently, the stability of the optimized gel is adequate for pharmaceutical applications, although incorporating stabilizers could potentially enhance its long-term storage capabilities [59].

At near-neutral pH, a decrease in the surface charge magnitude is expected, which could impact long-term stability. These nano-structural features likely enhanced permeation and enabled complete diffusion-controlled release *in vitro*. The drug release studies confirmed a full diffusion-controlled release over 24 h, fitting the Korsmeyer–Peppas model, with F7 achieving the highest cumulative release (98.86±0.24%). The release followed a first-order kinetic model (R^2 = 0.9864), indicating concentration-dependent release. The Korsmeyer-Peppas analysis (n = 0.7907) suggested a non-Fickian diffusion mechanism, likely due to combined drug diffusion and polymer chain relaxation effects. Similar diffusion-controlled release patterns have been documented in related systems: for example, a hydrogel incorporating Aloe vera-derived AgNPs showed>90% cumulative release over 24-36 h [60], and *Ficus benghalensis*, AgNP formulation achieved similarly high release *in vitro* [61]. Therefore, the release kinetics observed in our study were consistent with those reported for other phytogel systems.

The optimized phytogel (F7) exhibited significant antimicrobial activity, with inhibition zones comparable to those of standard antibiotics against Gram-positive and Gram-negative bacteria, as well as fungi. This wide-ranging activity is due to the inherent antimicrobial characteristics of *FV-BE* and the well-known

bactericidal effects of AgNPs. The synergistic effect likely results from the combined action of phytochemicals from *F. virens* bark and AgNPs. Previous research on herbal AgNPs, such as those from *Azadirachta indica, Ocimum sanctum,* and *Ficus religiosa*, has also shown improved antimicrobial effectiveness compared to formulations containing only silver. For instance, *A. indica and F. religiosa* AgNPs displayed potent antibacterial activity against both g-positive and g-negative strains, with a zone of inhibition comparable to standard antibiotics in some cases [62]. Compared to our optimized *FVBE*-AgNPs phytogel, which exhibited broad-spectrum antimicrobial activity, *O. sanctum* AgNPs nanogels also demonstrated zones similar to a marketed silver nitrate gel, despite using a lower silver concentration. Our results reinforce this evidence, emphasizing the role of secondary metabolites in enhancing antimicrobial efficacy [63].

The enhanced effectiveness compared to a commercial silver nanogel, even when accounting for silver content, indicated that the phytogel efficiently harnesses the bioactive compounds of *F. virens*. Stability tests conducted over three months under different storage conditions showed the durability of the formulation, with only slight variations in key parameters such as pH, entrapment efficiency, and drug content. This stability is crucial for preserving the shelf life and therapeutic efficacy. Similar stability profiles were noted in AgNPs-nanogel systems formulated with extracts from *Tridax procumbens* and other medicinal plants (*Musa balbisiana*, *Azadirachta indica, Ricinus communis*, *and Cardiospermum halicacabum*) topical gel [64-65], which retained acceptable pH, spreadability, good viscosity, and physicochemical properties during storage, further confirming that gel formulations with plant extracts can maintain>90 % of their functional attributes over extended periods. In our study, the optimized phytogel demonstrated broad antimicrobial activity, comparable to *Tridax procumbens* AgNPs, which produced inhibition zones of up to 21 mm against *S. aureus* and 23 mm against *P. aeruginosa* [64]. This supports the role of plant phytochemicals in enhancing the antibacterial efficacy of AgNPs, which is consistent with our *FV-BE* formulation.

These results are consistent with the existing research on combining plant extracts with nanocarriers to enhance antimicrobial action and improve topical delivery. The developed phytogel is a promising nanocarrier-based system that utilizes the natural bioactivity of *F. virens,* enhanced by nanotechnology, for potential topical antimicrobial treatments. *In vitro* results are encouraging; additional *in vivo* studies are needed to evaluate the effectiveness, safety, and pharmacokinetics of the formulation in a biological context. Furthermore, long-term stability assessments and testing for skin irritation or sensitization would be beneficial for clinical use. In conclusion, this study demonstrates the successful development of a stable and effective transdermal phytogel incorporating *FV-BE* and AgNPs. This optimized formulation offers a new approach to topical antimicrobial therapy by harnessing the synergistic effects of phytochemicals and nanotechnology. Further research, including *in vivo* experiments and clinical trials, are necessary to fully understand its therapeutic potential and safety profile.

CONCLUSION

A transdermal phytogel incorporating *Ficus virens* bark extract (*FV-BE*) and silver nanoparticles (AgNPs) was successfully created and refined for stability and effectiveness. Systematic analysis revealed that the concentration of Carbopol 940 and the amount of AgNPs significantly influenced the physicochemical and release characteristics of the formulation. This study successfully developed and optimized a novel phytogel formulation incorporating silver nanoparticles (AgNPs) and *Ficus virens* bark extract (FV-BE) for topical antimicrobial use. The optimized formulation (F7) containing 0.75% w/w Carbopol 940 and 0.02% w/w AgNPs with *FV-BE* exhibited desirable physicochemical properties, including suitable viscosity, spreadability, pH, high entrapment efficiency, and drug content. The formulation demonstrated complete diffusion-controlled release over 24 h, following a first-order kinetic model with a non-Fickian diffusion mechanism. The phytogel showed notable antimicrobial activity against both *Gram-positive* and *Gram-negative* bacteria, as well as fungi, with inhibition zones comparable to standard antibiotics. This broad-spectrum activity is attributed to the synergistic effect of *FV-BE* phytochemicals and AgNPs. Stability studies confirmed the formulation's robustness under various storage conditions over three months. While *in vitro* results are promising, further research, including *in vivo* experiments and clinical trials, is necessary to fully understand the therapeutic potential and safety profile of this formulation. The developed phytogel represents a promising nanocarrier-based system that harnesses the natural bioactivity of *F. virens*, enhanced by nanotechnology, for potential topical antimicrobial treatments.

ACKNOWLEDGEMENT

The authors express their sincere gratitude to the Institute of Pharmaceutical Sciences, Kurukshetra University, Kurukshetra, Haryana, India, for providing the facilities and support necessary to conduct this research.

FUNDING

This research received no external funding.

AUTHORS CONTRIBUTIONS

All authors contributed significantly to this work. Deepika Aggarwal: prepared the manuscript draft, performed data analysis and interpretation; Kamal Saroha and Manjusha Choudhary: Conceptualization, Supervision; Kamal Kaushik: Statistical analysis of data, review, and editing. All authors reviewed, edited, and approved the final version of the manuscript.

CONFLICT OF INTERESTS

The authors declare that there are no competing interests associated with this manuscript.

REFERENCES

1. Patil PB, Datir SK, Saudagar RB. A review on topical gels as drug delivery system. J Drug Delivery Ther. 2019 May 2;9(3-s):989-94. doi: 10.22270/jddt.v9i3-s.2930.
2. Bhuyan C, Saha D, Rabha B. A brief review on topical gels as drug delivery system. J Pharm Res Int. 2021 Oct 26;33(47A):344-57. doi: 10.9734/jpri/2021/v33i47A33020.
3. Alberti I, Grenier A, Kraus H, Carrara DN. Pharmaceutical development and clinical effectiveness of a novel gel technology for transdermal drug delivery. Expert Opin Drug Deliv. 2005 Sep 1;2(5):935-50. doi: 10.1517/17425247.2.5.935, PMID 16296788.
4. Nidhi A. Bagmar, Pooja R. Hatwar, Prashant G. Shelke, Ravindra L. Bakal. A review on "Topical gels: an emerging drug delivery system". GSC Biol PharmSci. 2024;28(2):285-96. doi: 10.30574/gscbps.2024.28.2.0311.
5. Sivadasan D, Madkhali OA. The design features, quality by design approach, characterization, therapeutic applications, and clinical considerations of transdermal drug delivery systems-A comprehensive review. Pharmaceuticals (Basel). 2024 Oct 9;17(10):1346. doi: 10.3390/ph17101346, PMID 39458987.
6. Jakasaniya P, Patel J, Dudhat K, Mori D. Formulation and optimization of gastro-retentive in situ gel of antiepileptic agent by using a Box–Behnken factorial design. Proc Indian Natl Sci Acad. 2025;91(1):285-98. doi: 10.1007/s43538-024-00343-5.
7. Amgaonkar YM, Kochar NI, Chandewar AV, Umekar MJ, Wadher KJ. Boswellic acid Loaded Nanoemulgel for Rheumatoid Arthritis: formulation Design and Optimization by QbD, *in vitro*, ex vivo, and *in vivo* evaluation. Ind J Pharm Edu Res. 2024 Apr 1;58(2):546-54. doi: 10.5530/ijper.58.2.61.
8. Saadh MJ, Mustafa MA, Kumar S, Gupta P, Pramanik A, Rizaev JA. Advancing therapeutic efficacy: nanovesicular delivery systems for medicinal plant-based therapeutics. Naunyn Schmiedebergs Arch Pharmacol. 2024 Oct;397(10):7229-54. doi: 10.1007/s00210-024-03104-9, PMID 38700796.
9. Ghosh B, Sarkar S, Ghosh S. Advancing sustainable wastewater treatment: unleashing the potential of nanosponges for effective remediation. In: Innovative and hybrid technologies for wastewater treatment and recycling. 2024. p. 381-404.
10. Dutta T, Barman A, Bhattacherjee S, Chakraborty J, Dutta T. Antimicrobial silver nanoparticles for water disinfection: a short review on recent advances. Nanotechnol Environ Eng. 2024 Mar;9(1):111-31. doi: 10.1007/s41204-023-00354-5.

11. Delgado Pujol EJ, Martinez G, Casado Jurado D, Vazquez J, Leon Barberena J, Rodríguez Lucena D. Hydrogels and nanogels: pioneering the future of advanced drug delivery systems. Pharmaceutics. 2025 Feb 7;17(2):215. doi: 10.3390/pharmaceutics17020215, PMID 40006582.
12. Modi DM, Modi AD. Nanogel-mediated therapeutic delivery across blood-cerebrospinal fluid and blood-spinal cord barriers. Brain Disord. Science Direct. 2024 Sep 1;15:100151. doi: 10.1016/j.dscb.2024.100151.
13. Herbig ME, Evers DH, Gorissen S, Köllmer M. Rational design of topical semi-solid dosage forms-how far are we? Pharmaceutics. 2023 Jun 26;15(7):1822. doi: 10.3390/pharmaceutics15071822, PMID 37514009.
14. Aggarwal D, Kamal CM, Agarwal G, Kumar A, Sharma D. Understanding of phyto-nanomedicine for the management of inflammation and wound healing: an outlook. Int J Pharm Sci Res. 2023 Oct;14(10):4713-23. doi: 10.13040/IJPSR.0975-8232.14(10).4713-23.
15. Simbine EO, Rodrigues LC, Lapa-guimaraes J, Kamimura ES, Corassin CH, Oliveira CA. Application of silver nanoparticles in food packages: a review. Food Sci Technol. 2019 Jun 27;39(4):793-802. doi: 10.1590/fst.36318.
16. Vijapur LS, Shalavadi M, Desai AR, Hiremath JN, Gudigennavar AS, Shidramshettar SL. Wound healing potential of green synthesized silver nanoparticles of *Glycyrrhiza glabra*Linn root extract: a preclinical study. J Trace Elem Min. 2025 Mar 1;11:100214. doi: 10.1016/j. jtemin.2025.100214.
17. Aldakheel FM, Sayed MM, Mohsen D, Fagir MH, El Dein DK. Green synthesis of silver nanoparticles loaded hydrogel for wound healing; systematic review. Gels. 2023 Jun 29;9(7):530. doi: 10.3390/gels9070530, PMID 37504410.
18. Odeniyi MA, Okumah VC, Adebayo-Tayo BC, Odeniyi OA. Green synthesis and cream formulations of silver nanoparticles of *Nauclea latifolia* (African peach) fruit extracts and evaluation of antimicrobial and antioxidant activities. Sustain Chem Pharm. 2020 Mar 1;15:100197. doi: 10.1016/j.scp.2019.100197.
19. Al-Ansari MM, Al-Dahmash ND, Ranjitsingh AJ. Synthesis of silver nanoparticles using gum arabic: evaluation of its inhibitory action on *Streptococcus mutans* causing dental caries and endocarditis. J Infect Public Health. 2021 Mar 1;14(3):324-30. doi: 10.1016/j.jiph.2020.12.016, PMID 33618277.
20. Mallineni SK, Sakhamuri S, Kotha SL, AlAsmari AR, AlJefri GH, Almotawah FN. Silver nanoparticles in dental applications: a descriptive review. Bioengineering (Basel). 2023 Mar 5;10(3):327. doi: 10.3390/bioengineering10030327, PMID 36978718.
21. Pandey AK, Harit AK, Sonekar K. Quantitative estimation of secondary metabolites, *in vitro* antioxidant, anti-inflammatory, and anti-sickling activity of leaf of *Ficus virens* Aiton. Int J Ayur Med. 2025;16(1):52-63. doi: 10.47552/ijam.v16i1.5317.
22. Saini Y, Kaushik K, Choudhary M, Bamrah PK, Choudhary N, Goyal A. Gastroprotective effect of ethanol extract of *Ficus virens* Aiton bark in ethanol induced *in vivo* ulcer model and exploring mechanism via molecular docking studies. Nutrire. 2025 Jun 2;50(1):42. doi: 10.1186/s41110-025-00341-7.
23. Ahmed S, Saifullah, Ahmad M, Swami BL, Ikram S. Green synthesis of silver nanoparticles using Azadirachta indica aqueous leaf extract. Journal of Radiation Research and Applied Sciences. 2016;9(1):1-7. doi: 10.1016/j.jrras.2015.06.006.
24. Saxena A, Tripathi RM, Zafar F, Singh P. Green synthesis of silver nanoparticles using aqueous solution of *Ficus benghalensis* leaf extract and characterization of their antibacterial activity. Mater Lett. 2012 Jan 15;67(1):91-4. doi: 10.1016/j.matlet.2011.09.038. matlet.2011.09.038.
25. Mihailovic V, Sreckovic N, Nedic ZP, Dimitrijevic S, Matic M, Obradovic A. Green synthesis of silver nanoparticles using *Salvia verticillata* and *Filipendula ulmaria* extracts: optimization of synthesis, biological activities, and catalytic properties. Molecules. 2023 Jan 13;28(2):808. doi: 10.3390/molecules28020808, PMID 36677866.
26. Singh C, Rao K, Yadav N, Bansal N, Vashist Y, Kumari S. A review: drug excipient Iincompatiblity by ftir spectroscopy. Curr Pharm Anal. 2023 Jun 1;19(5):371-8. doi: 10.2174/1573412919666230228102158.
27. Chadha R, Bhandari S. Drug-excipient compatibility screening – role of thermoanalytical and spectroscopic techniques. J Pharm Biomed Anal. 2014 Jan 18;87:82-97. doi: 10.1016/j.jpba.2013.06.016, PMID 23845418.
28. Rojek B, Wesolowski M. FTIR and TG analyses coupled with factor analysis in a compatibility study of acetazolamide with excipients. Spectrochim Acta A Mol Biomol Spectrosc. 2019 Feb 5;208:285-93. doi: 10.1016/j.saa.2018.10.020, PMID 30340208.
29. Aminu N, Chan SY, Mumuni MA, Umar NM, Tanko N, Zauro SA. Physicochemical compatibility studies of triclosan and flurbiprofen with excipients of pharmaceutical formulation using binary, ternary, and multi-combination approach. Futur J Pharm Sci. 2021 Jul 22;7(1):148. doi: 10.1186/s43094-021-00302-7.
30. Chen XX, Wu XB, Chai WM, Feng HL, Shi Y, Zhou HT. Optimization of extraction of phenolics from leaves of Ficus virens. J Zhejiang Univ Sci B. 2013 Oct;14(10):903-15. doi: 10.1631/jzus.B1200365. PMID 24101207.
31. Mahmoud MR, Mahgoub SM, Abdelazeem R, Abdelsatar MM, Allam AA, Alfassam HE. RP-HPLC method development and validation for the quantification of prednisolone and salbutamol with their simultaneous removal from water using modified clay–activated carbon adsorbents. RSC Adv. 2025;15(11):8675-95. doi: 10.1039/D5RA00324E, PMID 40114727.
32. Kaur SU, Kaur TA, Kaur GU, Verma SH. Development and validation of UV-spectrophotometric method for estimation of hydroquinone in bulk, marketed cream and prepared NLC formulation. Int J App Pharm. 2017 Sep;9(5):102-8. doi: 10.22159/ijap.2017v9i5.20467.
33. Makeen HA, Albratty M. Sesamol loaded silver nanoparticles gel engineered for wound healing via topical delivery: optimization *in vitro* and *ex vivo* evaluation. Curr Pharm Des. 2024 Dec;30(40):3175-89. doi: 10.2174/0113816128306956240801052553, PMID 39192646.
34. Aldakheel FM, Mohsen D, El Sayed MM, Fagir MH, El Dein DK. Green synthesized silver nanoparticles loaded in polysaccharide hydrogel applied to chronic wound healing in mice models. Gels. 2023 Aug 11;9(8):646. doi: 10.3390/gels9080646, PMID 37623101.
35. Wu X, Chen HW, Zhao ZY, Li L, Song C, Xiong J. Carbopol 940-based hydrogels loading synergistic combination of quercetin and luteolin from the herb Euphorbia humifusa to promote Staphylococcus aureus infected wound healing. RSC Med Chem. 2024;15(2):553-60. doi: 10.1039/D3MD00611E, PMID 38389873.
36. Budarapu D, Mohan Kumar U, Sravanthi P. Design, formulation and *in vitro* evaluation of ketoconazole microsponges by quasi-emulsion solvent diffusion method. J Drug Delivery Ther. 2025;15(7):19-24. doi: 10.22270/jddt.v15i7.7244.
37. Hassan H, Adam SK, Alias E, Meor Mohd Affandi MM, Shamsuddin AF, Basir R. Central composite design for formulation and optimization of solid lipid nanoparticles to enhance oral bioavailability of acyclovir. Molecules. 2021 Sep 7;26(18):5432. doi: 10.3390/molecules26185432, PMID 34576904.
38. Singh AP, Kashaw SK, Soni V. Design, optimisation and *in vivo* evaluation of tazarotene loaded emulgel formulation for the treatment of acne. J Drug Target. 2025 Aug 10:1-9. doi: 10.1080/1061186X.2025.2546489.
39. Desu PK, Karmakar B, Kondi V, Tiwari ON, Halder G. Optimizing formulation of green tea extract-loaded chitosan nanogel. Biomass Conv Bioref. 2024 Feb;14(3):3209-22. doi: 10.1007/s13399-022-02453-w.
40. Vandana D, Shweta Pawar. Formulation and evaluation of topical herbal gel containing inclusion complex of curcumin. Asian J Pharm Clin Res. 2019:196-201. doi: 10.22159/ajpcr.2019.v12i9.34053.
41. Alam MS, Algahtani MS, Ahmad J, Kohli K, Shafiq-un-Nabi S, Warsi MH. Formulation design and evaluation of aceclofenac nanogel for topical application. Ther Deliv. 2020 Dec 1;11(12):767-78. doi: 10.4155/tde-2020-0076, PMID 33225842.
42. Alam MS, Sultana N, Rashid MA, Alhamhoom Y, Ali A, Waheed A. Quality by design-optimized glycerosome-enabled nanosunscreen gel of rutin hydrate. Gels. 2023 Sep 15;9(9):752. doi: 10.3390/gels9090752, PMID 37754433.
43. Mhetre RL, Kagade AD, Dhole SN. Nanoemulgel for treatment of topical fungal infection: formulation and optimization using

box–behnken design. BioNano Science. 2025 Sep;15(3):1-4. doi: 10.1007/s12668-025-02121-z.

44. Avinash S, Gowda DV, Suresh J, Ram AS, Srivastava A, Osmani RM. Formulation and evaluation of topical gel using *Eupatorium glandulosum Michx*. for wound healing activity. Scholars Res Libr. 2016;8(8):255-66.
45. Lv Y, He H, Qi J, Lu Y, Zhao W, Dong X. Visual validation of the measurement of entrapment efficiency of drug nanocarriers. Int J Pharm. 2018 Aug 25;547(1-2):395-403. doi: 10.1016/j.ijpharm.2018.06.025, PMID 29894757.
46. Sodimalla T, Yalavarthi N. Biosynthesis of silver nanoparticles from *Pseudomonas fluorescens* and their antifungal activity against *Aspergillus niger* and *Fusarium udum*. Ann Appl Biol. 2022 Sep;181(2):235-45. doi: 10.1111/aab.12761.
47. Pandey S, Paul S, Jangde KK, Mishra DK. Development of sertaconazole loaded nanoemulgel using quality by design approach for enhanced antifungal drug delivery. J Pharm Innov. 2025 Oct;20(5):1-20. doi: 10.1007/s12247-025-10075-8.
48. Afreen U, Fahelelbom KM, Shah SN, Ashames A, Almas U, Khan SA. Formulation and evaluation of niosomes-based chlorpheniramine gel for the treatment of mild to moderate skin allergy. J Exp Nanosci. 2022 Dec 31;17(1):467-95. doi: 10.1080/17458080.2022.2094915.
49. Bhattacharya SA, Paul BI, Biswas GR. Development and evaluation of hydrogel of an anti-fungal drug. Int J Pharm Pharm Sci. 2023;15(10):29-33. doi: 10.22159/ijpps.2023v15i10.48728.
50. Jayachandran P, Ilango S, Suseela V, Nirmaladevi R, Shaik MR, Khan M. Green synthesized silver nanoparticle-loaded liposome-based nanoarchitectonics for cancer management: *in vitro* drug release analysis. Biomedicines. 2023 Jan 14;11(1):217. doi: 10.3390/biomedicines11010217, PMID 36672725.
51. Sadati Behbahani ES, Ghaedi M, Abbaspour M, Rostamizadeh K, Dashtian K. Curcumin loaded nanostructured lipid carriers: *in vitro* digestion and release studies. Polyhedron. 2019 May 15;164:113-22. doi: 10.1016/j.poly.2019.02.002.
52. Ahmadipour Z, Seyed Dorraji MS, Ashjari HR, Dodangeh F, Rasoulifard MH. Applying in-situ visible photopolymerization for fabrication of electrospun nanofibrous carrier for meloxicam delivery. Sci Rep. 2023 Jun 16;13(1):9741. doi: 10.1038/s41598-023-36893-9, PMID 37328688.
53. Pathan IB, Dwivedi R, Ambekar W. Formulation and evaluation of ketoprofen-loaded chitosan nanogel for pain management: *ex vivo* and *in vivo* study. Ars Pharm. 2019 Jun;60(2):101-8. doi: 10.30827/ars.v60i2.8563.
54. Mohammed GM, Hawar SN. Green biosynthesis of silver nanoparticles from *Moringa oleifera* leaves and its antimicrobial and cytotoxicity activities. Int J Biomater. 2022;2022(1):4136641. doi: 10.1155/2022/4136641, PMID 36193175.
55. Kabiru HD, Ahmad KB, Bello NM, Paul SO. Formulation and evaluation of *in vitro* antioxidant and antimicrobial activities of herbal hydrogel loaded with *Moringa oleifera* leaf extract. Sci World J. 2023 Apr 23;18(1):101-5. doi: 10.1371/journal.pone.0326858.
56. Martinez Higuera A, Rodriguez Beas C, Villalobos Noriega JM, Arizmendi Grijalva A, Ochoa Sanchez C, Larios Rodriguez E. Hydrogel with silver nanoparticles synthesized by *Mimosa tenuiflora* for second-degree burns treatment. Sci Rep. 2021 May 28;11(1):11312. doi: 10.1038/s41598-021-90763-w, PMID 34050228.
57. Aminu N, Alfred-Ugbenbo D, Moradeke O, Audu Mumuni M, Muhammad Umar N, Tanko N. Nanogel drug delivery system loaded with Azadirachta indica A. Juss. (Neem) for potential treatment of wound infection: development and characterization. Beni-Suef Univ J Basic Appl Sci. 2025 Jun 21;14(1):67. doi: 10.1186/s43088-025-00655-5.
58. Kumbhar S, Khairate R, Bhatia M, Choudhari P, Gaikwad V. Evaluation of curcumin-loaded chitosan nanoparticles for wound healing activity. ADMET DMPK. 2023 Oct 19;11(4):601-13. doi: 10.5599/admet.1897, PMID 37937244.
59. Chethan HV, Mohapatra D, SAHU A, Hemalatha S. Formulation development and evaluation of hydrogel containing silver nanoparticles with *Withania coagulans* aqueous extract. Indian J Pharm Sci. 2023 Jul 1;85(4). doi: 10.36468/pharmaceutical-sciences.1165.
60. Ragab A, El-Badry N, Tamer N, Naas A, Hamdy A, Tawakey SH. Biodegradable chitosan/PVA-based hydrogel incorporating green synthesized silver nanoparticles for wound healing applications. BMC Chem. 2025 Dec;19(1):190. doi: 10.1186/s13065-025-01564-5, PMID 40611305.
61. Din IU, Ajaj R, Rauf A, Ahmad Z, Muhammad N, Ali S. Ficus benghalensis extract mediated green synthesis of silver nanoparticles, its optimization, characterization, computational studies, and its *in vitro* and *in vivo* biological potential. PLOS One. 2025 Jul 1;20(7):e0326858. doi: 10.1371/journal.pone.0326858, PMID 40591582.
62. Buggana A, Bandari K, Golla N, Golla N, Abd-Elsalam KA. Leaf-mediated green synthesis of silver nanoparticles from *Azadirachta indica* and *Ficus religiosa*: characterization and bioactive properties. Egypt J Agric Res. 2024 Sep 1;102(3):392-406. doi: 10.21608/ejar.2024.285666.1541.
63. Sood R, Chopra DS. Optimization of reaction conditions to fabricate *Ocimum sanctum* synthesized silver nanoparticles and its application to nano-gel systems for burn wounds. Mater Sci Eng C Mater Biol Appl. 2018 Nov 1;92:575-89. doi: 10.1016/j.msec.2018.06.070, PMID 30184784.
64. Fatima F, Aldawsari MF, Ahmed MM, Anwer MK, Naz M, Ansari MJ. Green synthesized silver nanoparticles using *Tridax procumbens* for topical application: excision wound model and histopathological studies. Pharmaceutics. 2021 Oct 21;13(11):1754. doi: 10.3390/pharmaceutics13111754, PMID 34834169.
65. Rajurkar A, Gogri D, Jamdade N, Pathak A. Green synthesis of silver nanoparticles: their characterization, antimicrobial, antioxidant activity and nanogel formulation. Nano Biomed Eng. 2023 Mar 1;15(1):42-50. doi: 10.26599/NBE.2023.9290006.